Technical note

Investigation of active control of swept shock wave/turbulent boundary-layer interactions – PSP results

J. S. Couldrick, S. L. Gai, J. F. Milthorpe and K. Shankar
School of Aerospace, Civil and Mechanical Engineering
University College, UNSW
Australian Defence Force Academy,
Canberra, Australia

ABSTRACT

An investigation of active control of the swept shock wave/boundary-layer interaction using 'smart' flap actuators is presented. The actuators are manufactured by bonding piezoelectric material to an inert substrate to control the bleed/suction rate through a plenum chamber. The cavity provides communication of signals across the shock, allowing rapid thickening of the boundary layer approaching the shock. This splits the shock foot into a series of weaker shocks forming a lambda structure, thus reducing wave drag. Active control allows optimisation of the unimorph deflection, hence rate of mass transfer.

In this paper, results of the interaction using pressure sensitive paint (PSP) are emphasised. It is shown that the use of PSP, in conjunction with discrete pressure data, enables the main features of the interaction to be observed when the actuators are subject to different deflections.

NOMENCLATURE

I	illuminescence intensity
k	temperature dependant coefficient
L	streamline
M_n	normal Mach number
P	pressure
T	temperature

Subscripts

0	stagnation
ref	PSP reference picture

Abbreviations

ACSBLI	active control of SBLI
EDM	electro discharge machining
MS	main shock
PCSBLI	passive control of SBLI
PSP	pressure sensitive paint
PZT	lead zirconate titanate (piezoelectric)
SBLI	shock-wave–boundary-layer interaction
ULS	uncontrolled lambda structure

1.0 INTRODUCTION

For very weak shock waves, such as with an upstream Mach number of around 1·1, the extent of the sswept shock wave/boundary-layer interaction (SBLI) is relatively weak, allowing the normal shock wave to extend into the boundary layer virtually as far as the sonic line with little smearing[1-3]. However, as the upstream Mach number increases, the distortion of the shock foot due to boundary layer thickening becomes increasingly significant. Above an upstream

Paper No. 2884. Manuscript received 10 March 2004, revised version received 5 August 2004, accepted 23 August 2004.

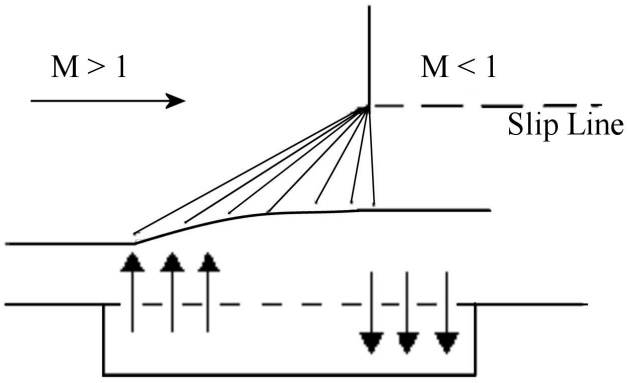

Figure 1. Passive control of the chock wave/boundary layer interaction (PCSBLI).

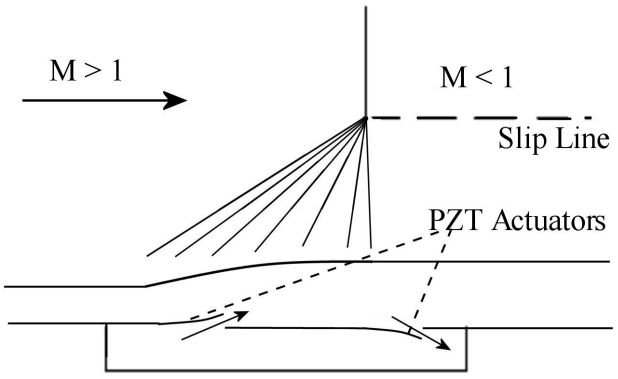

Figure 2. Active control of the shock wave/boundary-layer interaction (ACSBLI).

Mach number of around 1·3, incipient separation occurs and the shock wave foot bifurcates above the boundary layer to form a lambda (λ) foot[4-7]. The leading shock is usually highly oblique with the trailing part of the lambda foot nearly normal.

Previous work[8-17] has been to passively control the interaction by replacing the surface beneath the foot of the shock wave with a porous plate covering a plenum chamber, (Fig. 1). This allows high-pressure air from the flow downstream of the shock wave to re-circulate through the plenum chamber into the low-pressure flow upstream of the shock wave. The cavity provides communication of signals across the shock, allowing rapid thickening of the boundary layer approaching the shock. The shock then splits into a series of weaker shocks forming a lambda shock foot, thus reducing wave drag. Furthermore, the suction down-stream reduces separation and viscous losses.

Historically, active control of the shock wave/boundary-layer interaction (ACSBLI) has been hampered by the drag reduction achieved being negated by the additional drag due to the power requirements, for example, the pump in the case of mass transfer and the drag of the devices in the case of vortex generators. The object of the present research[18-24] is to assess the concept of active control using 'smart' flap actuators, (Fig. 2). The actuators are designed using PZT-5H piezoelectric material to control bleed/suction rate.

The plenum chamber pressure would approximately be at a mean pressure of the upstream and downstream pressure. Using this assumption, the pressure difference acting on the actuator will, therefore, be the difference between the chamber pressure and the free stream pressure.

Active control allows optimisation of the interaction by positioning the control region around the original shock position and by controlling the unimorph deflection and hence rate of mass transfer. Previous work[20] has structurally optimised the unimorph actuators. This paper presents the PSP results and how they can be used, along with discrete pressure data, to identify the main features of the swept SBLI. It should be noted that the current work does not include a closed loop system and the term active control is mainly used to signify that the magnitude of unimorph deflection, and therefore level of SBLI control, can be managed.

2.0 EXPERIMENTAL ARRANGEMENT

2.1 Wind-tunnel configuration

The work was carried out in a blow-down supersonic wind tunnel and a swept shock-wave–boundary-layer interaction was produced on the tunnel sidewall. An 11° wedge, mounted on the floor, in a Mach 2·0 free stream produces a swept shock with a normal shock Mach number (M_n) of 1·3 (Fig. 3(a)). For a static pressure in the test section of 44kPa the 'smart' flaps will then have a 17·64kPa pressure difference acting across them.

A plenum chamber (140mm × 20mm) is placed underneath the swept shock in the sidewall of the test section. The plenum chamber is covered by a plate containing the 'smart' flaps and numerous pressure ports, (Fig. 3(b)). The flaps were cut into the plate, by electro discharge machining (EDM), with a gap of 0·05mm between the model skin and the flap.

The piezo-ceramic is bonded to the underside of the flap and a voltage is applied to control the actuator deflection and thus mass transfer rate. The surface pressures were recorded using a single Druck PCD22 (3·5bar) pressure transducer that steps through the various ports using a scanivalve. Surface pressures were recorded in both streamwise and transverse directions, as shown in Fig. 3(c).

2.2 Pressure sensitive paints

Although PSPs are a relatively recent flow visualisation technique, they have been increasingly used in quantitative aerodynamic applications because of their ability to provide a picture of the instantaneous pressure field over entire surfaces without disturbing the flow[25].

PSP techniques are based on the deactivation of photochemically excited organic molecules, the so called luminophores, by oxygen molecules. This process is called 'oxygen quenching'. A luminophore is shifted to an excited electronic state (singlet) when it absorbs a photon of appropriate energy. This excited luminophore can return to the ground electronic state by emitting a photon (photoluminescence). It can also return to the ground state by a collision with an oxygen molecule. If this occurs, the oxygen absorbs the excess energy of the luminophore, and the transition to the ground state is radiationless. If, in a given volume, the number of oxygen molecules increases the chance of excited luminophores undergoing radiationless transfers increases; that is, the photoluminescence decreases[26].

Radiometric imaging was used to determine the global pressure distribution. It requires a calibration curve to be established before a pressure distribution can be determined from the images over the model. The pressure can be calculated using the ratio of the ambient pressure intensity and the intensity during a run. The rewritten Stern-Volmer equation is then given as.

$$p = k_1(T) + k_2(T)\left(\frac{I_{ref}}{I}\right) + k_3(T)\left(\frac{I_{ref}}{I}\right)^2 \quad \ldots (1)$$

where I_{ref} and I are the intensities at ambient pressure and during the run. k_1, k_2 and k_3 are temperature dependent constants.

https://doi.org/10.1017/S0001924000000300 Published online by Cambridge University Press

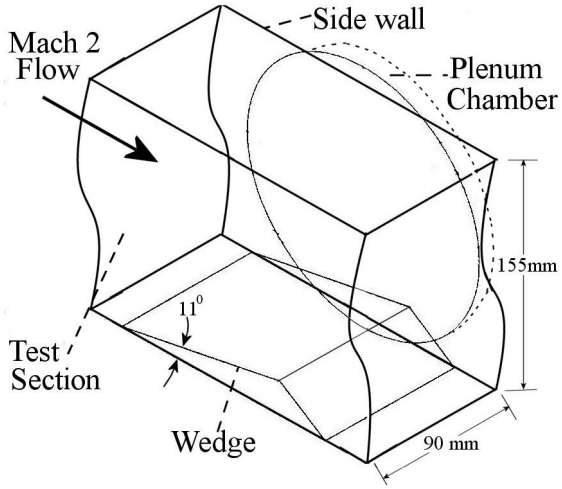

(a)

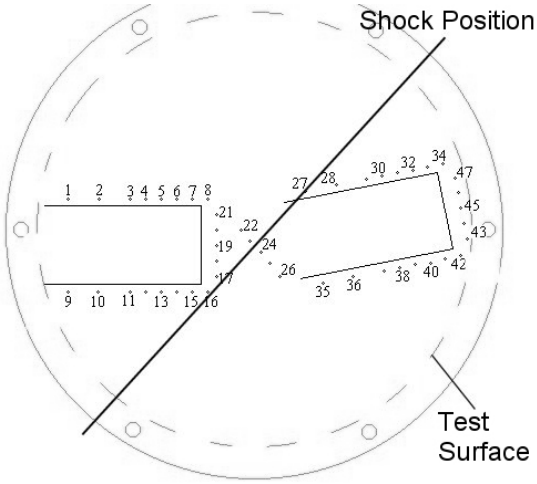

(b)

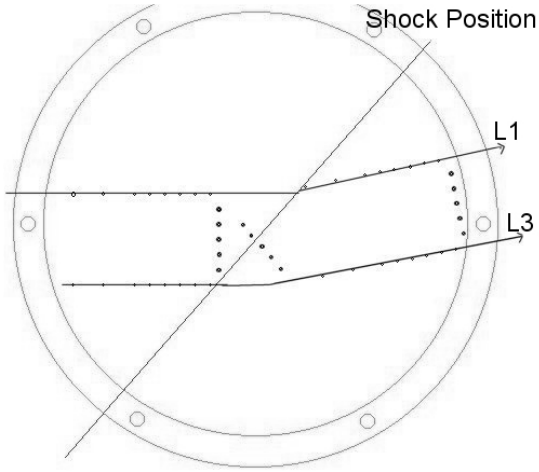

(c)

Figure 3 (a). Wedge flush to the tunnel floor and shown in relation to the test section, (b) pressure port layout on test surface and (c) measurement co-ordinate system.

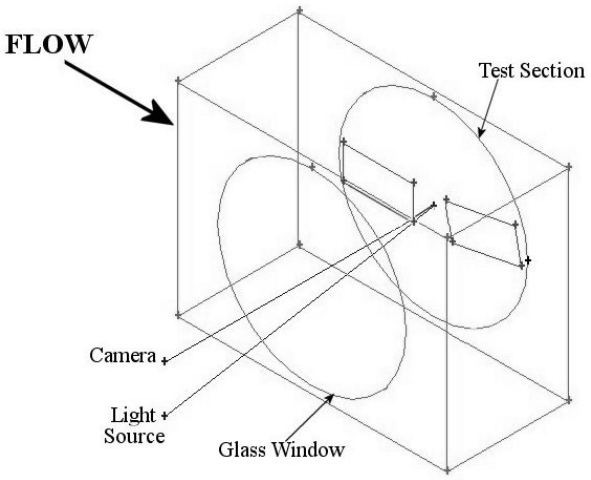

Figure 4. Camera/test surface/light source set-up.

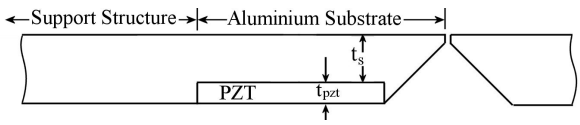

Figure 5. Modified unimorph flap configuration.

A Unicoat aerosol PSP Pt(TfPP) with a response time of less than a second was utilised for ease of application combined with a UV LED 464nm light source, (Fig. 4). The camera is perpendicular to the test surface and due to logistics the light source is positioned 10° lower and downstream of the camera. The angle of the light source creates a crescent shadow on the lower downstream test surface, which creates pressure noise in the imaging process in the shadow region.

3.0 UNIMORPH ACTUATOR DESIGN

The concept for the unimorph set-up was to have the piezoceramic embedded within the surface material, (Fig. 5), to allow a greater bonding area and improved deflection properties, whilst retaining a flush upper surface. A lip was then incorporated into the design to minimise the deflection required before mass transfer occurred.

Total unimorph tip deflection can be considered as the combination of the deflection due to the acting pressure and the piezoelectric deflection. The piezoelectric deflection can assist or inhibit unimorph deflection depending on the polarity of the applied voltage.

The unimorph deflection varies with the substrate's Young's Modulus and thickness. The selection of substrate is a trade-off between suppressing the deflection due to the pressure difference across the flap, whilst keeping the unimorph piezoelectrically flexible to create active control. Active control of the shock boundary layer interaction requires that the flaps are able to close, that is to have zero deflection and minimum mass transfer, to be regarded as capable of active control.

The optimal substrate material/thickness was calculated using a combination of finite element modelling and composite laminar plate theory[20,23]. The aluminium unimorph substrate is 52mm long, 25mm wide and 0·9mm thick. It was hoped to achieve better piezoelectric performance in testing than theory suggests due to the assumption of a constant mean pressure within the plenum

https://doi.org/10.1017/S0001924000000300 Published online by Cambridge University Press

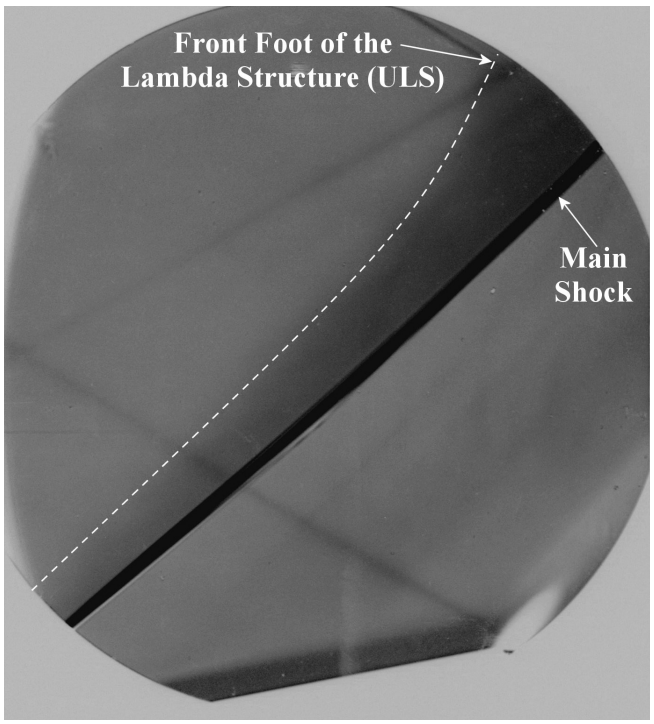

Figure 6. Negative greyscale rendering of colour schlieren of the uncontrolled SBLI.

chamber. In reality, there will be a pressure gradient in the plenum and spillage around the side edges, which will reduce the pressure acting on the flaps.

4.0 RESULTS

4.2.1. Uncontrolled swept SBLI

Referring to Figure 6, the flow is from left to right, with the main shock at approximately 41° to the main flow direction. With an 11° wedge and a shock normal Mach number of 1·3, the flow would be incipiently separated according to Korkegi's criterion[7]. Also, according to Kubota and Stollery[6], for a freestream Mach number of 2, incipient separation occurs for a wedge angle between 10° and 12° so that the present flow is on the verge of separation. It is observed that this is, indeed, the case as the main shock is smeared at the tunnel wall as indicated by the darker region upstream of the main shock. The dashed white line marks the approximate start of this darker region which indicates the foot of the leading edge of the uncontrolled lambda structure (ULS)[1,20,27]. The foot of the lambda structure line is seen to initially diverge from the swept shock angle by approximately 4·5°, which agrees with the trend of Alvi and Settles work on swept interaction without control[1]. This divergence angle is observed to increase as the swept shock interacts with both wall and ceiling boundary layers[2].

A localised region of low pressure exists above the wedge as the flow is expanded over the top of the wedge. Furthermore, two shocks can be observed that originate far upstream of the test section. They are believed to be relatively weak as there is no apparent hue change either side of them. It is assumed that the expansion fan and the weak shocks will not significantly influence the discrete pressure data and PSP results.

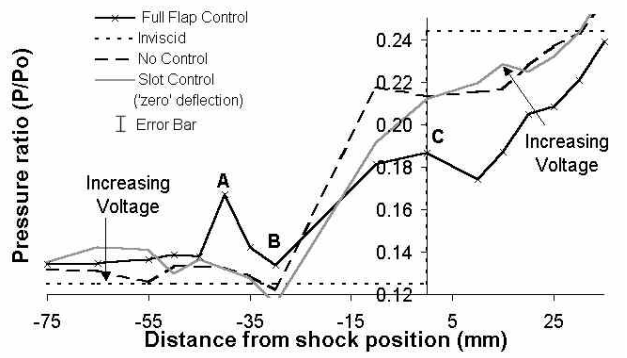

(a)

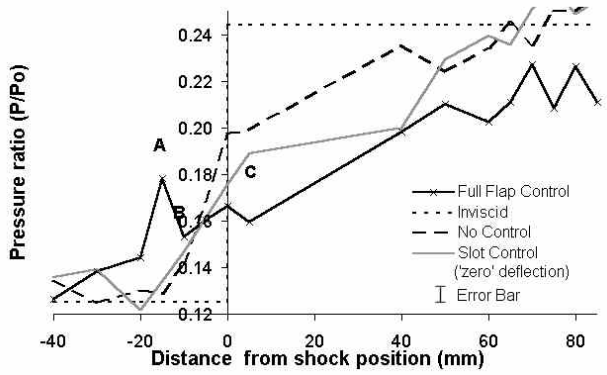

(b)

Figure 7. Surface pressures along (a) *L*1 and (b) *L*3 as shown by Couldrick[20].

4.2.2 Actuator SBLI control[20]

Figures 7 (a) and (b) show the pressure distribution for swept shock wave/boundary-layer interaction control along *L*1 and *L*3. They describe flap control using 'smart' flaps with the trend shown for increasing voltage; showing no control, slot control to indicate zero flap deflection and full flap control (500V). Distances are shown from the calculated wedge shock position with a negative distance implying upstream, (Fig. 3(c)). The discrete pressure data, as shown in Figs 7(a) and (b), has an accuracy of $\pm 0{\cdot}003 p/P_0$.

This discrete pressure data shows that unimorph flap actuators provide a degree of beneficial control of the shock wave/boundary-layer interaction. The full flap control produces a larger lambda structure as indicated by the local pressure maximum (*A*) and the lower pressure plateau (*C*) as compared to the no control and slot control (zero unimorph deflection) cases. However, Figs 7. (a) and (b) would also suggest that unimorph actuators could not provide 'real' active control as the pressure distribution (using 500V) with zero unimorph deflection is different from the no control distribution. This indicates that a form of control is still present when voltage is applied and the control is not 'turned off.' This is presumably due to some leakage across the 0·05mm gap between the model skin and the flap, creating continuous longitudinal slot control.

4.3 Pressure sensitive paint (PSP)

Values of I_{ref}/I were obtained by taking a reference image of the model at atmospheric pressure ('wind off') and an image when

https://doi.org/10.1017/S0001924000000300 Published online by Cambridge University Press

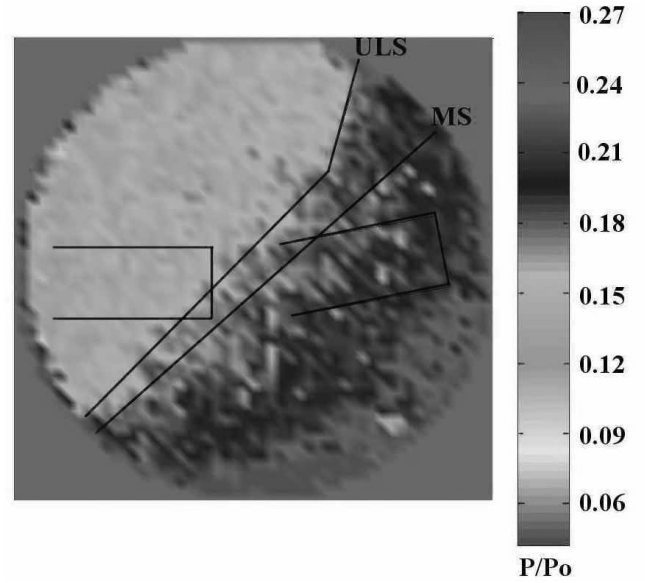

Figure 8. Greyscale rendering of pressure distribution map of the uncontrolled SBLI using PSP.

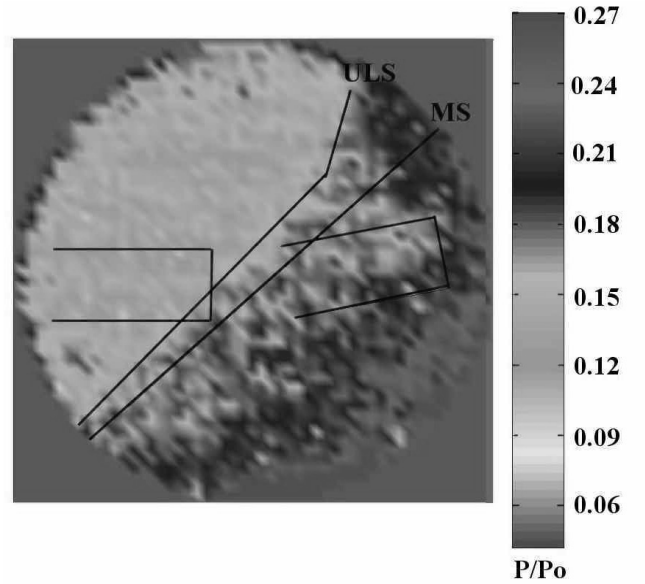

Figure 9. Greyscale rendering of pressure distribution map of unimorph control with 500V applied voltage using PSP.

the tunnel was running ('wind on'). The pressure distribution was then determined from the calibration equation (Equation 1). The coefficients, k_1, k_3 and k_3, were calculated using measured pressure data and intensity ratios at numerous locations, (Fig. 3(b)). The images were processed using MATLAB® by breaking the images into 576*720 matrices of intensities and then averaging over 4 × 4 element (1mm × 1mm) 'tiles' to attempt to reduce the noise in the data. The reduction of noise is a trade off with high-resolution information, providing an accuracy of ±0·02 p/P_0. The positions of the unimorph flaps, main shock (MS) and the front foot of the uncontrolled lambda structure (ULS), as calculated from Fig. 6, have been overlaid on the processed figures for ease of comparison, (Figs 8, 9, 11 and 12).

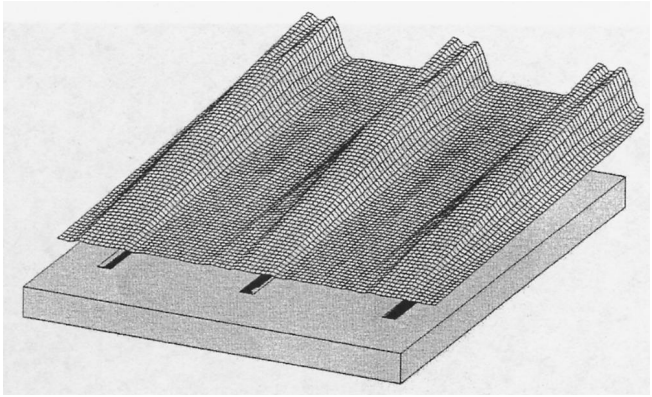

(a)

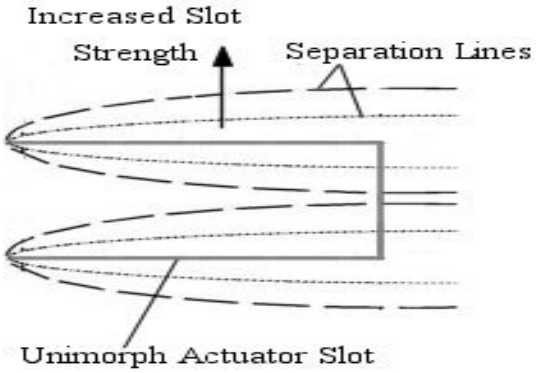

(b)

Figure 10 (a). 3D 'bubbles of influence' of slot control of the SBLI and (b) the effect of slot strength[29].

PSP was applied over the circular test surface (Fig. 3(a)) and the experiments were conducted at approximately 0°C ±2°C, which is the flow adiabatic wall temperature to minimise any heat transfer between the flow and the control plate. As indicated by equation 1, the luminescence of the paint is temperature dependent so any heat transfer will produce spurious results. The luminescence is then recorded by a digital camera and post-processed.

Furthermore, it is believed that a crescent of approximately 10% of the test section area in the bottom right hand section of the picture is indicating higher pressure than actual due to the shadowing effects of the light angle to the test section, (Fig. 4) as discussed in Section 2.2. However, it is not precisely known to what extent this effect occurs but it is known that it does not extend as far as the downstream unimorph.

4.3.1 Uncontrolled SBLI

Figure 8 is observed to closely agree with the schlieren picture taken for the location of the leading edge of the uncontrolled lambda structure (Fig. 6). Furthermore, it is in close agreement with the discrete pressure data obtained (Figs 7(a) and (b)). It is also observed that the pressure upstream of the uncontrolled lambda structure is somewhat uniform and increases to a mean pressure as it travels through the lambda structure. Downstream of the shock wave/boundary-layer interaction the pressure further

https://doi.org/10.1017/S0001924000000300 Published online by Cambridge University Press

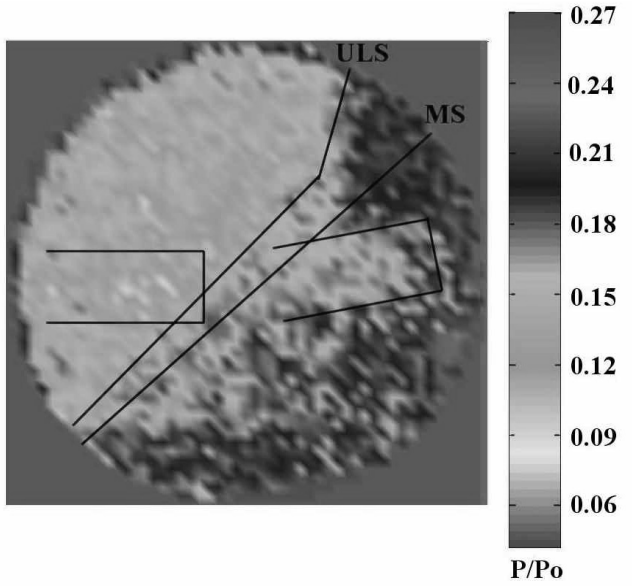

Figure 11. Greyscale rendering of pressure distribution map of unimorph control with 0V applied voltage using PSP.

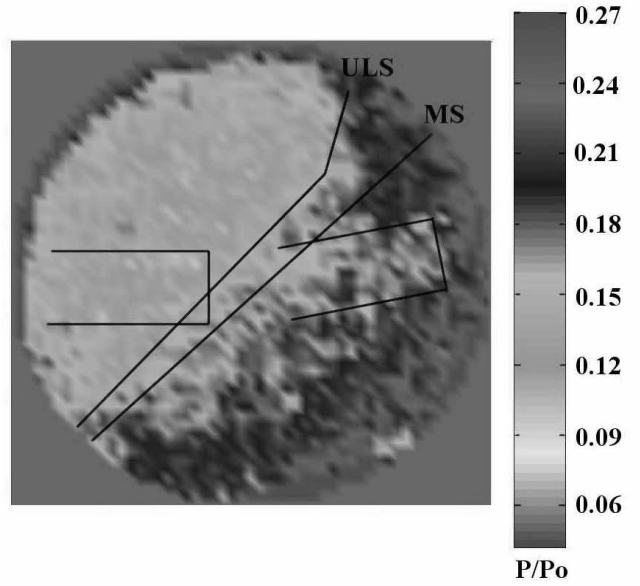

Figure 12. Greyscale rendering of pressure distribution map of unimorph control with –500V applied voltage using PSP.

rises and achieves approximate inviscid levels as it reaches the end of the control plate. The lesser region of lower pressure that is observed at the bottom right of the picture is generated by the flow expanding over the wedge.

4.3.2 'Closed' unimorph (500V)

It was theoretically calculated that zero deflection should be achievable with a 500V applied voltage across the piezoceramic[20]. Figure 9 shows the surface pressure distribution map using a 500V applied voltage. A distinct pressure rise across the position of the leading foot of the uncontrolled lambda structure position can be seen with minimal extra smearing compared to the uncontrolled pressure distribution map (Fig. 8). This indicates that the global flow field is approximately uncontrolled and the extra smearing observed, especially over the down stream unimorph, is expected to be due to the limited localised passive slot control produced.

A slight pressure drop towards the sides of the upstream unimorph, is believed to be due to localised expansion as a result of boundary layer thickening caused by the interaction control provided by the streamwise slot effect, as a result of seepage across the actuator as discussed in Section 4.2.2. Similar flow features are also seen in the slot control of SBLIs studied by Smith *et al*[28,29]. This slot control effect can be considered the result of a 3D bubble forming just upstream of the slot position and expanding with downstream distance, (Fig. 10(a)).

The 'bubble of influence' dissipates into the global flow field at distances away from the slot position. It is thought that the size of the bubble, located on top of the separation line, is related to the size and strength of the control region, (Fig. 10(b)). However, the slot effect is minimal due to the size of the slots as compared with the approximate 7mm thickness of the incoming boundary layer. The work of Smith *et al* had slot widths of the order of the boundary-layer thickness where as the present work has slot widths two orders of magnitude less than the boundary layer thickness.

4.3.3 'Uncontrolled' unimorph (0V)

Figure 11 shows the interaction with a 0V applied voltage across the piezoceramic producing an uncontrolled unimorph SBLI. The unimorph tip deflection achieved is a product of the pressure difference only. It should be noted that there is increased noise due to the trade off with resolution, as discussed in Section 4.3.

The leading edge of the lambda structure is not seen to have significantly moved but a higher degree of smearing can be observed, compared to the closed flaps (500V) case, and therefore would imply a reduction in wave drag. The smearing has spread below the unimorph region as the larger lambda structure has an increased influence on the neighbouring flow field, which requires a finite time to merge back into the lambda structure of an uncontrolled SBLI. However, in the top right hand section of the test surface the pressure rise is sharper as the leading foot of the lambda structure is seen to diverge more, becoming increasingly normal to the flow.

Furthermore, the low-pressure region on the upstream unimorph flap has increased in area, with a decreased pressure, as the slot control 'bubbles of influence' have grown due to the increase in mass injection/slot control strength as a result of increased unimorph deflection.

4.3.4 'Fully deflected' unimorph (-500V)

An increase in unimorph deflection should be theoretically achieved with a negative applied voltage. A –500V voltage was applied to the piezoceramics to observe the interaction, (Fig. 12).

Again, the leading edge of the lambda structure is observed not to have appreciably moved and the shock smearing observed is similar to that observed with a 0V applied voltage. There is a similar termination of the lambda structure, in the top right hand section of Fig. 12, but there is reduced shock smearing in the neighbouring lower flow field. However, it is not known whether this is a reduced noise effect or the increased unimorph tip deflection producing larger/stronger slot control, which creates a stronger terminating leg of the lambda structure in the neighbouring flow field.

The low-pressure region on the upstream unimorph has increased uniformity, with a reduced pressure compared to the 0V

https://doi.org/10.1017/S0001924000000300 Published online by Cambridge University Press

and 500V cases. This suggests the stronger slot control is producing larger 'bubbles of influence' above the upstream unimorph.

4.3.5 Flap deflection effects

In the above discussion, the effects of unimorph deflection, per se, have not been mentioned. Indeed, there will be effects due to an upstream compression ramp and downstream expansion corner. However, with the amount of deflection being less than 1mm in a 52mm length of the unimorphs, it is expected that the deflection effects will be at least an order of magnitude less than the mass transfer effects. Furthermore, this deflection will create non-linearity in the PSP intensity recorded by the camera but it is expected that such discrepancies would be far outweighed by the noise in the pressure sensitive paint imaging.

5.0 CONCLUSIONS

Experiments have shown that SBLI control using piezoelectric actuators is feasible. Although a constant average pressure between the upstream (low pressure) and downstream (high pressure) was assumed, there is, in reality, a pressure gradient in the plenum chamber and spillage will occur around the edge of the actuators, where the flow escapes through the gaps between the model skin and the flap, thus reducing the pressure acting on the actuators.

From the discrete pressure data obtained, the concept of piezoelectric actuator flap control is shown to be an effective method of controlling the shock wave/boundary-layer interaction. However, the unimorph actuators were unable to completely eliminate the 'control' effects.

Using the discrete pressure data, in conjunction with the PSP, it is seen that the pressure distribution is more complicated and the pressure maps obtained show that, globally, active control is achieved with unimorph flaps. However, the presence of slots control gives a locally continuous passive control of the interaction.

It was assumed that with a 500V applied voltage the unimorph flaps are closed and have zero deflection. The pressure distribution map however, indicates that the global flow field is approximately uncontrolled with a small amount of extra smearing, resulting in a limited localised passive slot control.

When the unimorphs are free to deflect, with 0V applied voltage, the leading edge of the lambda structure is not seen to change significantly. However, a higher degree of smearing can be observed, compared to the 'flaps closed' case, indicating thereby a broader lambda shock structure and hence implying a reduction in wave drag.

With a –500V applied voltage, to assist unimorph deflection, the leading edge of the lambda structure is observed not to move appreciably and the shock smearing is similar to that observed with a 0V applied voltage. However, it is not known whether the increased unimorph tip deflection, from 0V to –500V, produces improved slot control or if the increased deflection has exceeded the optimum amount for control.

REFERENCES

1. ALVI, A. and SETTLES, G.S. Physical model of the swept shock wave boundary-layer interaction flowfield, *AIAA J,* 1992, **30**, (9), pp 2252-2258.
2. GREEN, J.E. Interactions between shock waves and turbulent boundary layers, *Progress in Aerospace Science*, (1969), **11**, pp 253-340.
3. KOIDE, S., SAIDA, N. and OGATA, R. Correlation of separation angles induced by glancing iteractions, *AIAA J*, 1996, **34**, (10 Technical Notes), pp 2198-2200.
4. ATKIN, C.J., and SQUIRE, L.C. A study of the interaction of a normal shock wave with a turbulent boundary layer at Mach numbers between 1·30 and 1·55, *Eur J Mech, B/Fluids*, 1992, **11**, (1), pp 93-118.
5. INGER, G.R. Application of a shock-turbulent boundary layerinteraction theory in transonic flowfield analysis, 1981, AIAA Transonic Perspective Symposium, 18-20 February 1981, NASA/Ames Research Center, Moffett Field, California, USA.
6. KUBOTA, H. and STOLLERY, J.L. An experimental study of the interaction between a glancing shock wave and a turbulent boundary layer, *J Fluid Mechanics*, 1982, **116**, pp 431-458.
7. SETTLES, G.S. and DOLLING, D.S. Swept shock-wave/boundary layer interactions, *Progress in Astronautics and Aeronautics*, 1992, **141**, (SEEBASS, A.R., Ed), pp 505- 574.
8. BABINSKY, H. Control of swept shock wave/turbulent boundary-layer interactions, 1999, ISSW22, July 18-23 1999, Imperial College, London.
9. BAHI, L., ROSS, J.M. and NAGAMATSU, H.T. Passive shock wave/boundary-layer control for transonic airfoil drag reduction, 1983, AIAA 21st Aerospace Sciences Meeting, January 1983, Reno, Nevada, USA.
10. GIBSON, T.M., BABINSKY, H. and SQUIRE, L.C. Passive control of shock wave/boundary-layer interactions, *Aeronaut J*, 2000, **104**, (1033), pp 129-140.
11. NAGAMATSU, H.T., FICARRA, R.V. and DYER, R. Supercritical airofoil drag reduction by passive shock wave/boundary-layer control in the Mach number range ·75 to ·90, 1985, AIAA 23rd Aerospace Sciences Meeting, January 1985, Reno, Nevada, USA.
12. NAGAMATSU, H.T., MITTY, T.J. and NYBERG, G.A. Passive shock wave/boundary-layer control of a helicopter rotor airfoil in a contoured transonic wind tunnel, 1987, AIAA 25th Aerospace Sciences Meeting, January 1987, Reno, Nevada, USA.
13. RAGHUNATHAN, S. Effects of porosity strength on passive shock-wave/boundary layer control, *AIAA J*, 1987, **25**, (5), pp 757-758.
14. RAGHUNATHAN, S. Passive control of shock-boundary layer interaction, Progress in Aerospace Science, 1988, **25**, pp 271-296.
15. RAGHUNATHAN, S., GRAY, J.L. and COOPER, R.K. Effects of inclination of holes on passive shock wave boundary layer control, 1987, AIAA 25th Aerospace Sciences Meeting, January 1987, Reno, Nevada, USA.
16. RAGHUNATHAN, S. and MABEY, D.G. Passive shock-wave/boundary layer control on a wall-mounted model, *AIAA J*, 1987, **25**, (2), pp 275-278.
17. SAVU, G. and TRIFU, O. Porous airfoils in transonic flow, *AIAA J*, 1984, **22**, (7 Technical Notes), pp 989-991.
18. COULDRICK, J.S., GAI, S., MILTHORPE, J. and SHANKAR, K. Development of 'smart' flap actuators for swept shock wave boundary layer interaction control, 2001, Australian International Aerospace Conference, Canberra, Australia.
19. COULDRICK, J.S., GAI, S., MILTHORPE, J. and SHANKAR, K. Swept shock wave boundary layer interaction control with 'smart' flap actuators, 2002, 40th AIAA Aerospace Sciences Meeting and Exhibition, January 2002, Reno, Nevada, USA.
20. COULDRICK, J.S., GAI, S., MILTHORPE, J. and SHANKAR, K. Active control of swept shock wave/turbulent boundary layer interactions, *Aeronaut J*, 2004, **108**, (1080), pp 93-101.
21. COULDRICK, J.S., GAI, S.L., MILTHORPE, J. and SHANKAR, K. Swept and normal shock wave/turbulent boundary layer interaction control with 'smart' flap actuators, 2003, CEAS Aerospace Aerodynamics Research Conference, 10-12 June 2003, RAeS, London, UK.
22. COULDRICK, J.S., SHANKAR, K., GAI, S. and MILTHORPE, J. Design optimisation of 'smart' flap actuators for swept shock wave boundary layer interaction control, 2002, 2nd Advances in Structural Engineering and Mechanics, 21-23 August 2002, Pusan, Korea.
23. COULDRICK, J.S., SHANKAR, K., GAI, S. and MILTHORPE, J. Design of 'smart' flap actuators for swept shock wave/turbulent boundary layer interaction control, *Structural Engineering and Mechanics: An International Journal*, 2003, **16**, (5), pp 519-532.
24. COULDRICK, J.S., SHANKAR, K., GAI, S. and MILTHORPE, J. Structural design of 'smart' actuator flaps for control of shock wave boundary layer interactions, 2003, Advanced Technology in Experimental

https://doi.org/10.1017/S0001924000000300 Published online by Cambridge University Press

Mechanics, 10-12 September 2003, Nagoya, Japan.
25. MORRIS, M.J., DONOVAN, J.F., KEGELMAN, J.T., SCHWAB, S.D. and LEVY, R.L. Aerodynamic applications of pressure sensitive paint, *AIAA J,* 1993, **31**, (3), pp 419-425.
26. KLEIN, C. Application of pressure sensitive paint (PSP) for the determination of the instantaneous pressure field of models in a wind tunnel, *Aerospace Science Technology*, 2000, **4**, pp 103-109.
27. SQUIRE, L.C. Interaction of swept and unswept normal shock waves with boundary layers, *AIAA J*, 1996, **34**, (10), pp 2099-2101.
28. SMITH, A.N., BABINSKY, H., DHANAESEKARAN, P.C., SAVILL, A.M. and DAWES, W.N. Computational investigation of slot and groove controlled shock wave/boundary-layer interactions, 2003, AIAA Paper 03-0446, 41st AIAA Aerospace Sciences Meeting and Exhibition, 6-9 January 2003, Reno, Nevada, USA.
29. SMITH, A.N., BABINSKY, H., FULKER, J.L. and ASHILL, P.R. Normal shock wave/turbulent boundary layer interactions in the presence of streamwise slots and gtrooves, *Aeronaut J*, 2002, **106**, (1063), pp 493-500.